Current-Limiting Droop Control of Grid-Connected Inverters

Qing-Chang Zhong, *Fellow, IEEE*, and George C. Konstantopoulos, *Member, IEEE*

***Abstract*—A current-limiting droop controller is proposed for single-phase grid-connected inverters with an *LCL* filter that can operate under both normal and faulty grid conditions. The controller introduces bounded nonlinear dynamics and, by using nonlinear input-to-state stability theory, the current-limiting property of the inverter is analytically proven. The proposed controller can be operated in the set mode to accurately send the desired power to the grid or in the droop mode to take part in the grid regulation, while maintaining the inverter current below a given value at all times. Opposed to the existing current-limiting approaches, the current limitation is achieved without external limiters, additional switches, or monitoring devices and the controller remains a continuous-time system guaranteeing system stability. Furthermore, this is achieved independently from grid voltage and frequency variations, maintaining the desired control performance under grid faults as well. Extensive experimental results are presented to verify the droop function of the proposed controller and its current-limiting capability under normal and faulty grid conditions.**

***Index Terms*—Current-limiting property, droop control, fault ride through, inverter, nonlinear stability.**

I. Introduction

POWER systems stability has been an active area of research for many decades. However, recently, the large-scale integration of renewable energy sources to the power network has started to significantly affect the stable and reliable operation of the grid. This has created essential requirements for grid-connected units to contribute to the stability of the grid by assisting in the regulation of the grid voltage and frequency. Droop control is often used to enhance the stability of power systems dominated by grid-connected inverters without requiring any communication among the different units [1]–[3]. In the most common scenario, inverters have a multiloop control structure with an inner current controller followed by a voltage controller that is adjusted through the desired droop functions [4].

Droop control has different forms when the impedance involved has a different type [1], [5], [6]. For example, when the impedance is inductive, which is the most common case nowadays, the droop control takes the form of $P \sim \omega$ and $Q \sim V$. When the impedance is resistive, e.g., in low-voltage networks or inverters with resistive output impedance [7]–[9], the droop control takes the form of $P \sim V$ and $Q \sim -\omega$. When the impedance is capacitive [5], [10], the droop control takes the form of $P \sim -\omega$ and $Q \sim -V$. Droop control has been extensively studied in the literature for both grid-connected and islanded operation of inverters [1], [11]–[13]. Several control methods have been developed to improve the droop control performance, such as the addition of an extra phase shift term [14], adapting the controller parameters using a grid-impedance estimator [15], or changing the output impedance of the inverter [3], [16], [17]. Among these methods, the robust droop controller reported in [16] not only can achieve the desired droop functions but can also guarantee tight output voltage regulation near the rated value independently from parameter variations or external disturbances. It was originally proposed for inverters having a dominantly resistive output impedance but it has recently been shown that this robust droop controller is actually universal for inverters having an output impedance with a phase angle between $-\frac{\pi}{2}$ and $\frac{\pi}{2}$ rad [6]. Hence, it will be adopted in this paper.

The stability of droop control methods have been extensively investigated in the literature, by using the small-signal modeling of the system and linearization methods [18]–[21]. However, the stability of droop-controlled inverters that include the nonlinear model of the closed-loop system have not been adequately demonstrated, partially due to the high complexity of the nonlinear dynamics resulted from the nonlinear expressions of the real and the reactive power. Recently, nonlinear analysis has been conducted in order to strengthen the stability theory [22]–[25]. In most of the existing stability approaches, several assumptions have been considered such as a purely inductive network or constant load and line impedances, while the inner voltage and current control loops are often neglected for the analysis [26].

Another issue about grid-connected inverters is to maintain the current below a given maximum limit. At the moment, most grid-connected converters are current controlled and therefore the current-limiting property is not a problem, but these converters lack of the capability of voltage regulation, which is a

Manuscript received May 4, 2016; revised July 15, 2016 and September 2, 2016; accepted October 9, 2016. Date of publication October 27, 2016; date of current version June 9, 2017. This work was supported by the Engineering and Physical Sciences Research Council (EPSRC), U.K., under Grant EP/J01558X/1. *(Corresponding author: Qing-Chang Zhong.)*

Q.-C. Zhong was with the Department of Automatic Control and Systems Engineering, The University of Sheffield, Sheffield, S1 3JD, U.K. He is now with the Department of Electrical and Computer Engineering, Illinois Institute of Technology, Chicago, IL 60616, USA (e-mail: zhongqc@ieee.org).

G. C. Konstantopoulos is with the Department of Automatic Control and Systems Engineering, The University of Sheffield, Sheffield, S1 3JD, U.K. (e-mail: g.konstantopoulos@sheffield.ac.uk).

Color versions of one or more of the figures in this paper are available online at http://ieeexplore.ieee.org.

Digital Object Identifier 10.1109/TIE.2016.2622402

crucial aspect of power-electronics-enabled autonomous power systems. It is important for every voltage controlled, in particular, droop controlled, distributed generation unit to possess a current-limiting property in a completely decentralized manner, which should be maintained at all times during both normal and abnormal grid conditions, i.e., during grid faults [27]–[30]. Fault current-limiting controllers can be applied to achieve the desired current limitation by either triggering suitably designed protection circuits [29], [31], [32] or by using several low-voltage ride-through structures [33], [34], which will continue injecting power to the grid with a limited current. Several of these methods are based on algorithmic control schemes and lack from a rigorous stability proof. Additionally, external limiters and saturation units are often added into the current or voltage loop control loops to achieve the desired current-limiting property, but these approaches can lead to undesired oscillations and instability [35]–[37]. A controller for grid-connected inverters that partially overcomes these limitations has been recently reported in [38], based on a bounded control structure [39], but only unity power factor can be accomplished. Hence, the reactive power could not be controlled and remains always close to zero. This clearly indicates that the droop functions cannot be implemented. Hence, the design of droop-controlled inverters with an inherent current limitation, considering the nonlinear dynamic model of the system, represents a challenging task.

A current-limiting droop control strategy for single-phase grid-connected inverters is proposed in this paper using the nonlinear dynamic model description. The inverter is assumed to be connected to the grid through an *LCL* filter, where the grid is assumed stiff or at least with bounded voltage and frequency close to their rated values. First, a generic control structure consisting of two voltage terms, one of which can be controlled, and a dynamic virtual resistance is formulated. Then, inspired by the form of the universal robust droop controller [6], [16], these terms are defined accordingly to design a current-limiting droop controller. By incorporating input-to-state stability analysis, it is analytically proven that the inverter current always remains below a given value. In this way, the advantages of the universal robust droop controller including the tight capacitor voltage regulation are maintained with an additional function to limit the inverter current below a given value, thus protecting the inverter and the filter at all times. Additionally, no external limiters or monitoring systems are required for limiting the inverter current, with the current limiting being an inherent property of the proposed controller as it is mathematically proven for the nonlinear closed-loop system. To complete the design procedure, a guidance for selecting the controller parameters and several comments regarding the practical implementation are also presented. It is also shown that the current-limiting property is guaranteed independently from grid voltage and frequency variations, extending the application of the controller to grid-fault cases. With comparison to [38], a generic control structure is proposed to achieve both current-limiting and droop control. Moreover, the proposed approach can control both the real and the reactive power of the inverter, providing the opportunity to switch between two operating modes for grid-connected inverters: i) real and reactive power regulation to reference values and ii) droop control. Extensive experimental results are provided to verify the current-limiting property of the proposed controller as well as its performance for different operating modes of the grid-connected inverter under both normal and faulty grid conditions.

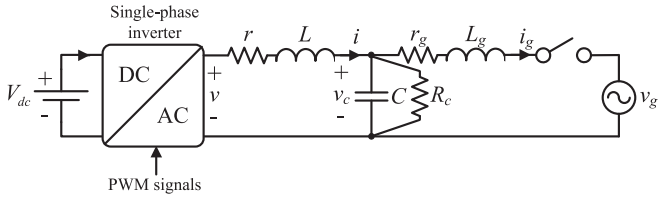

Fig. 1. A grid-connected single-phase inverter with an LCL filter.

II. Dynamic Modeling and Problem Formulation

Fig. 1 shows the system under consideration. It consists of a single-phase inverter connected to the grid via an LCL filter. The LCL filter inductances are denoted as L and L_g with small parasitic resistances in series r and r_g, respectively, and the filter capacitor is given by C with a large parasitic resistance R_c in parallel. The inverter output voltage and current are v and i, respectively. v_c is the capacitor voltage, and v_g and i_g are the grid voltage and current, respectively. Initially, the grid is considered stiff with $v_g = \sqrt{2}V_g \sin\omega_g t$, where V_g is the RMS grid voltage and ω_g is the grid angular frequency, although later the main result is extended to cases where the grid voltage and frequency might vary from their rated values.

The dynamic model of the system is given as

$$\begin{aligned} L\frac{di}{dt} &= -ri + v - v_c \\ C\frac{dv_c}{dt} &= i - \frac{v_c}{R_c} - i_g \\ L_g\frac{di_g}{dt} &= v_c - r_g i_g - v_g \end{aligned} \tag{1}$$

which is a linear dynamic system with state vector $x = [i \quad v_c \quad i_g]^T$, while v_g represents an uncontrolled external input. The control input is the inverter voltage v.

In order for the inverter to support the grid voltage and frequency regulation, droop control is adopted in the control design, where the control input takes the form of $v = \sqrt{2}E\sin\theta$ with $\dot{\theta} = \omega$ being the angular frequency of the inverter. Although several droop control methods have been proposed in the literature, as outlined and explained in the Section I, this paper adopts the robust universal droop controller [6], [16] in the form of

$$\omega = \omega^* + m(Q - Q_{\text{set}}) \tag{2}$$

$$\dot{E} = K_e(E^* - V_c) - n(P - P_{\text{set}}) \tag{3}$$

where ω^* and E^* are the rated angular frequency and voltage, respectively, K_e is a positive constant gain, V_c is the RMS value of the capacitor voltage, P_{set} and Q_{set} correspond to the reference values of the real and the reactive power, and n and m are the droop coefficients. The measured real and reactive power P and Q are usually obtained at the capacitor node as the average values of the instantaneous power expressions over

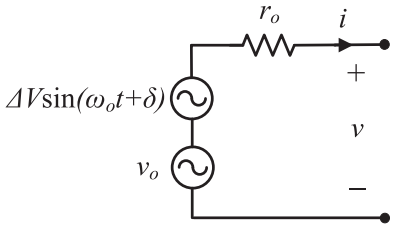

Fig. 2. Equivalent circuit diagram of the controller.

a period T, which for a single-phase inverter become

$$P = \frac{1}{T}\int_t^{t+T} v_c(\tau)i(\tau)d\tau,\ Q = \frac{1}{T}\int_t^{t+T} v_{cq}(\tau)i(\tau)d\tau \quad (4)$$

where v_{cq} is the capacitor voltage delayed by $\frac{\pi}{2}$ rad. It is then obvious that the power expressions are nonlinear due to the multiplication of the system states, resulting in a nonlinear closed-loop system that is difficult to analyze in terms of stability.

The purpose of the proposed paper is to develop a droop control scheme that inherits the advantages of the robust droop controller and limits the inverter current under a given value, based on the nonlinear dynamic model of the closed-loop system.

III. Controller Design and Analysis

A. Controller Structure

For grid-connected inverters, the inverter RMS voltage E and the phase θ are often controlled to obtain the inverter voltage $v = \sqrt{2}E\sin\theta$. The output impedance can be controlled to be resistive, which improves the power quality and enhances the stability of the system, especially under grid voltage variations [1], [7]. In this case, the inverter voltage v is subtracted by a term $r_o i$, where r_o is the virtual resistance and i is the inverter current, thus forming the R-inverter as noted in [1]. In this section, the focus is on the design of the virtual resistance to obtain the desired current-limiting property. In order to achieve this, a generic controller for grid-connected inverters is proposed in the following form:

$$v = v_o + \Delta V\sin(\omega_o t + \delta) - r_o i \quad (5)$$

which consists of a base voltage v_o, a controllable voltage source $\Delta V\sin(\omega_o t+\delta)$, and a dynamic virtual resistance r_o. Here, v_o, ΔV, ω_o, δ, and r_o should be controlled to achieve different operating modes, realizing the droop control functions (2) and (3) and the crucial current-limiting property. The equivalent circuit of the controller is shown in Fig. 2.

B. Controller Design

For the design of a current-limiting droop controller, the controller (5) is designed to have:

1) $v_o = v_c$;
2) $\Delta V = \sqrt{2}(1-w_q)V_g$;
3) $\omega_o = \omega_g$;
4) $r_o = (1-w_q)w$.

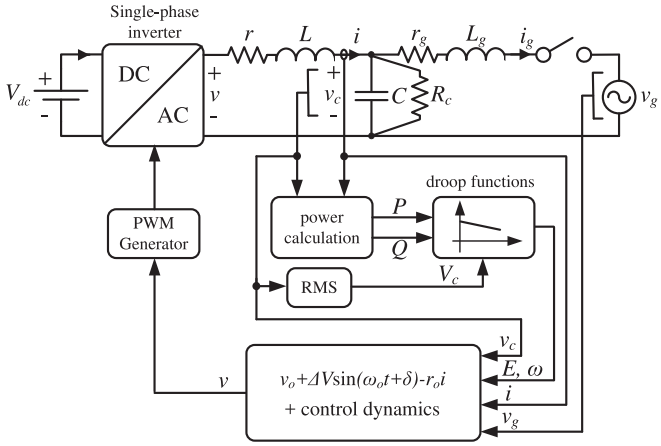

Fig. 3. Overall control system.

with the controller taking the form

$$v = v_c + (1-w_q)(\sqrt{2}V_g\sin(\omega_g t+\delta) - wi). \quad (6)$$

Here, the variables w, w_q, and δ are designed to dynamically change in order to introduce the droop functions and they have to be bounded within given sets to guarantee the stability and the desired current-limiting property. For example, since $r_o = (1-w_q)w$ is a virtual resistance, it has to be positive and larger than a minimum value. Considering the desired droop function expressions in (2) and (3) and the bounded controller described in [39], the dynamics of the controller states w, w_q, δ, and δ_q are designed as

$$\dot{w} = -c_w\left(K_e(E^*-V_c) - n(P-P_{\text{set}})\right)w_q^2 \quad (7)$$

$$\dot{w}_q = \frac{c_w(w-w_m)w_q}{\Delta w_m^2}\left(K_e(E^*-V_c) - n(P-P_{\text{set}})\right) - k_w\left(\frac{(w-w_m)^2}{\Delta w_m^2} + w_q^2 - 1\right)w_q \quad (8)$$

$$\dot{\delta} = c_\delta\left(\omega^* - \omega_g + m(Q-Q_{\text{set}})\right)\delta_q^2 \quad (9)$$

$$\dot{\delta}_q = -\frac{c_\delta\delta\delta_q}{\Delta\delta_m}\left(\omega^* - \omega_g + m(Q-Q_{\text{set}})\right) - k_\delta\left(\frac{\delta^2}{\Delta\delta_m^2} + \delta_q^2 - 1\right)\delta_q \quad (10)$$

with c_w, c_δ, w_m, Δw_m, $\Delta\delta_m$, k_w, and k_δ being positive constants. The initial conditions of w, w_q and δ, δ_q are defined as $w_0 = w_m$, $w_{q0} = 1$ and $\delta_0 = 0$, $\delta_{q0} = 1$, respectively. Note that both V_g and ω_g can be obtained using a traditional phase-locked loop (PLL). The overall control system is shown in Fig. 3. Note that the universal robust droop control principle (2) and (3) are embedded in the controller dynamics and hence it is a droop controller. Moreover, the virtual resistance r_o is dynamically controlled according to the $P\sim V$ droop and the phase shift δ in the controllable voltage source is dynamically controlled according to the $Q\sim -\omega$ droop. Hence, in order to

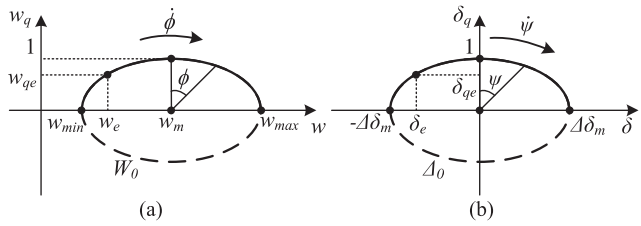

Fig. 4. Controller states w, w_q and δ, δ_q on the $w - w_q$ and $\delta - \delta_q$ planes, respectively.

guarantee system stability, these terms should be proven to remain bounded, which is explained below.

For system (7) and (8), by considering the Lyapunov function candidate

$$W = \frac{(w - w_m)^2}{\Delta w_m^2} + w_q^2 \tag{11}$$

its time derivative yields

$$\dot{W} = \frac{2(w - w_m)\dot{w}}{\Delta w_m^2} + 2w_q\dot{w}_q.$$

By substituting $\dot{w}$ and $\dot{w}_q$ from (7) and (8), respectively, $\dot{W}$ can be found, after some calculations, as

$$\dot{W} = -2k_w\left(\frac{(w - w_m)^2}{\Delta w_m^2} + w_q^2 - 1\right)w_q^2. \tag{12}$$

According to the initial conditions w_0 and w_{q0}, both w and w_q start and stay at all times on the ellipse

$$W_0 = \left\{w, w_q \in R : \frac{(w - w_m)^2}{\Delta w_m^2} + w_q^2 = 1\right\}$$

as shown in Fig. 4(a), because on W_0 there is

$$\dot{W} = 0 \Rightarrow W(t) = W(0) = 1 \quad \forall t \geq 0.$$

By choosing $w_m > \Delta w_m > 0$, the ellipse is defined on the right half plane, resulting in $w \in [w_{\min}, w_{\max}] = [w_m - \Delta w_m, w_m + \Delta w_m] > 0$ for all $t \geq 0$. Now, define the transformation

$$w = w_m + \Delta w_m \sin\phi, \text{ and } w_q = \cos\phi. \tag{13}$$

Note that the term $-k_w(\frac{(w-w_m)^2}{\Delta w_m^2} + w_q^2 - 1)w_q$ in (8) is zero on the ellipse W_0. Then by substituting (13) into (7) and (8), after some calculations, there is

$$\dot{\phi} = \frac{-c_w\left(K_e(E^* - V_c) - n(P - P_{\text{set}})\right)w_q}{\Delta w_m} \tag{14}$$

which means that the states w and w_q travel on the ellipse W_0 with angular velocity $\dot{\phi}$. When $K_e(E^* - V_c) = n(P - P_{\text{set}})$, the robust droop controller settles down in the steady state and $\dot{\phi} = 0$. Hence, w and w_q converge to some constant values w_e and w_{qe}, respectively, corresponding to the desired equilibrium point.

Note that by starting from point $(w_m, 1)$ on the $w - w_q$ plane, the controller states w and w_q are restricted only on the upper semiellipse of W_0. This is due to the fact that the angular velocity $\dot{\phi}$ depends on w_q from (14), since if the states try to reach the horizontal axis, then $w_q \to 0$ and $\dot{\phi} \to 0$ independently from the term $K_e(E^* - V_c) - n(P - P_{\text{set}})$. This forces the controller states to slow down and remain on the upper semiellipse of W_0, avoiding a continuous oscillation around W_0. Therefore, it holds true that $w_q \in [0, 1]$ for all $t \geq 0$.

Similarly, the controller states δ and δ_q in (9) and (10) operate exclusively on the upper semiellipse of

$$\Delta_0 = \left\{\delta, \delta_q \in R : \frac{\delta^2}{\Delta\delta_m^2} + \delta_q^2 = 1\right\}$$

with angular velocity

$$\dot{\psi} = \frac{c_\delta\left(\omega^* - \omega_g + m(Q - Q_{\text{set}})\right)\delta_q}{\Delta\delta_m} \tag{15}$$

and similar properties as described above, resulting in $\delta \in [-\Delta\delta_m, \Delta\delta_m]$ and $\delta_q \in [0, 1]$ for all $t \geq 0$, as shown in Fig. 4(b). Thus, all controller states w, w_q, δ, and δ_q are proven to remain bounded for all $t \geq 0$.

The proposed controller can be operated in different modes. In the steady state, $\dot{w} = 0$ and $\dot{\delta} = 0$, which means the controller achieves the droop function given in (7)–(10). By removing the term $K_e(E^* - V_c)$ from (7) and (8) and the term $\omega^* - \omega_g$ from (9) and (10), the controller can be operated in the set mode to achieve power flow control so that accurate real and reactive power can be sent to the grid. This allows a simple change of the operating modes of the inverter from the droop mode to the set mode at any time. In fact, this is one of the main differences of the proposed controller compared to the one in [38]. The control structure (6), together with the control dynamics (7)–(10), allow the regulation of both the real and the reactive power as well as the implementation of droop functions, but the approach in [38] can only achieve unity power factor.

C. Current-Limiting Property

By applying the proposed controller (6) into the original plant dynamics (1), the inverter current equation becomes

$$L\frac{di}{dt} = -(r + (1 - w_q)w)\,i + (1 - w_q)\sqrt{2}V_g\sin(\omega_g t + \delta). \tag{16}$$

From the previous controller analysis, it holds true that $w \in [w_{\min}, w_{\max}] > 0$ and $w_q \in [0, 1]$ for all $t \geq 0$. Then, for system (16), consider the Lyapunov function candidate

$$V = \frac{1}{2}Li^2. \tag{17}$$

It represents the energy stored in the inductor L. Its time derivative is

$$\begin{aligned}\dot{V} &= -(r + (1 - w_q)w)\,i^2 + (1 - w_q)\sqrt{2}V_g i\sin(\omega_g t + \delta)\\ &\leq -(r + (1 - w_q)w_{\min})\,i^2\\ &\quad + (1 - w_q)\sqrt{2}V_g\,|i|\,|\sin(\omega_g t + \delta)|\,.\end{aligned}$$

This shows that $\dot{V} < 0$ when $|i| > \frac{(1-w_q)\sqrt{2}V_g|\sin(\omega_g t+\delta)|}{r+(1-w_q)w_{\min}}$, proving that (16) is input-to-state stable (ISS) [40]. Since $(1 -$

$w_q)\sqrt{2}V_g \sin(\omega_g t+\delta)$ is bounded, then the inverter current i is bounded for all $t \geq 0$. According to the ISS property, it holds true that

$$|i| \leq \frac{(1-w_q)\sqrt{2}V_g}{r+(1-w_q)w_{\min}} \quad \forall t \geq 0$$

if initially $i(0)$ satisfies the previous inequality. By choosing

$$w_{\min} = \frac{V_g}{I_{\max}} \tag{18}$$

then

$$|i| \leq \frac{(1-w_q)}{r\frac{I_{\max}}{V_g}+(1-w_q)}\sqrt{2}I_{\max} < \sqrt{2}I_{\max} \tag{19}$$

since $(1-w_q) \geq 0$ and $r\frac{I_{\max}}{V_g} > 0$. The previous inequality holds for any $t \geq 0$ and for any constant positive $I_{\max}$. As a result

$$I < I_{\max} \quad \forall t \geq 0$$

where I is the RMS value of the inverter current, proving that the proposed controller introduces an inherent current-limiting property independently from the droop function, the nonlinear expressions of P, Q, V_c and the dynamics of δ. This is a crucial property since the inverter is protected at all times by limiting the output current, even if a large reference value P_{set} is applied.

It is possible to find a different Lyapunov function candidate, which results in a different limit for the current. However, it is impossible to find a Lyapunov function candidate to obtain a limit lower than $I_{\max}$ through the choice of $w_{\min}$ from (18) because the closed-loop system (16) is an *RL* circuit with a voltage source. Note that the actual limit of I depends on the small parasitic resistance r. As it can be seen from (19), when the value of r is significant (not zero), the maximum limit of the current will reduce. However, the current-limiting property below $I_{\max}$ is still guaranteed and this holds independently from the filter, i.e., without requiring any knowledge of the inductor L and its parasitic resistance r.

D. Closed-Loop Stability

It has been shown above that the controller states and the filter inductor current always remain bounded. In order to investigate the stability of the rest of the plant states, the dynamics of the capacitor voltage and the grid current in (1) can be re-written as

$$\begin{bmatrix} \frac{dv_c}{dt} \\ \frac{di_g}{dt} \end{bmatrix} = \begin{bmatrix} -\frac{1}{R_c C} & -\frac{1}{C} \\ \frac{1}{L_g} & -\frac{r_g}{L_g} \end{bmatrix} \begin{bmatrix} v_c \\ i_g \end{bmatrix} + \begin{bmatrix} \frac{i}{C} \\ -\frac{v_g}{L_g} \end{bmatrix} \tag{20}$$

which can be seen as a linear time-invariant system of the form $\dot{x} = Ax + u$ with state $x = [\,v_c \quad i_g\,]^T$ and input $u = [\,\frac{i}{C} \quad -\frac{v_g}{L_g}\,]^T$. By choosing

$$P = \begin{bmatrix} C & 0 \\ 0 & L_g \end{bmatrix} > 0$$

it can be found that

$$PA + A^T P = \begin{bmatrix} -\frac{2}{R_c} & 0 \\ 0 & -2r_g \end{bmatrix} < 0$$

which proves that A is Hurwitz and (20) is a bounded-input bounded-state stable system. Since $v_g = \sqrt{2}V_g \sin\omega_g t$ is bounded and i is bounded from the ISS and the current-limiting properties, both the capacitor voltage v_c and the grid current i_g are proven to remain bounded at all times.

The virtual resistance r_o introduced by the controller, as shown in Fig. 2, is in series with the filter inductor L, which is equivalent to increasing the parasitic resistance r of the inductor L or adding a resistor in series with the filter inductor. Hence, it is able to enhance the damping of the system.

E. Selection of the Controller Parameters

Since the term $(1-w_q)w$ represents a dynamic virtual resistance at the output of the inverter and $w_{\min}$ corresponds to the maximum current $I_{\max}$, similarly, the initial value $w_0 = w_m$ can be determined by the given initial current I_m as

$$w_m = \frac{V_g}{I_m}.$$

Note that initially, when the inverter is not connected to the grid, a small amount of current still flows through the *LC* filter. In particular, since the RMS capacitor voltage is almost at V_g to have a smooth connection ($v_c \approx v_g$), then the inverter current before the connection will be

$$I_m = \omega^* C V_g.$$

As a result, w_m can be chosen as

$$w_m = \frac{1}{\omega^* C}. \tag{21}$$

According to the ellipse W_0, the parameter Δw_m is given as

$$\Delta w_m = w_m - w_{\min} = \frac{1}{\omega^* C} - \frac{V_g}{I_{\max}}. \tag{22}$$

The parameter $\Delta\delta_m$ corresponds to the maximum absolute value of δ. According to (16), the controller state δ describes the phase shifting applied to the inverter voltage. By neglecting the small phase shifting applied by the filter inductor L, the value of δ corresponds to the reactive power of the inverter, i.e., $\delta = 0$ and $\delta = -\frac{\pi}{2}$ will approximately correspond to $Q = 0$ and $Q = S_n$, respectively, where S_n is the rated power of the inverter. Therefore, $\Delta\delta_m$ is chosen as $\frac{\pi}{2}$ in order to control the reactive power in the range $Q \in [-S_n, S_n]$. In practice, $\Delta\delta_m$ can be chosen slightly smaller to cope with the small inductance L.

Parameters k_w and k_δ should be arbitrary positive constants since they are multiplied with the terms $\frac{(w-w_m)^2}{\Delta w_m^2} + w_q^2 - 1$ and $\frac{\delta^2}{\Delta\delta_m^2} + \delta_q^2 - 1$ in (8) and (10), which are zero on the ellipses W_0 and Δ_0, respectively. In fact, these terms are used to increase the robustness of the w_q and δ_q dynamics in an actual implementation due to calculation errors or external disturbances.

Parameters c_w and c_δ are found in the angular velocities (14) and (15) of the controller states, respectively. The selection of c_w is discussed at first. Since w and w_q start from point $(w_m, 1)$, they travel on the ellipse W_0 and can reach the point $(w_{\min}, 0)$ at the limit of the current after a settling time t_s, then by considering the worst case scenario where the controller states travel on the arc of W_0 with central angle $\frac{\pi}{2}$ rad and with a maximum angular velocity $\frac{\pi}{2t_s}$ rad/s, one can calculate a minimum value of c_w. Since tight voltage regulation can be achieved for the capacitor voltage ($V_c \approx E^*$) and $w_q \leq 1$, assuming the real power starts from zero and reaches the maximum real power $P_{\text{set}} = S_n$, then from (14) it yields

$$\dot{\phi}_{\max} = \frac{\pi}{2t_s} = \frac{c_w n S_n}{\Delta w_m}$$

which finally gives

$$c_w = \frac{\pi \Delta w_m}{2t_s n S_n}. \tag{23}$$

Similarly, parameter c_δ can be determined as

$$c_\delta = \frac{\pi \Delta \delta_m}{2t_s m S_n}. \tag{24}$$

Note that both (23) and (24) provide some guidance for selecting c_w and c_δ only because they are obtained for the worst case scenario. In practice, larger values can be chosen or equivalently smaller t_s can be used.

F. Practical Implementation

Since during the grid-connected operation, in most applications L_g and r_g are relatively small, the small phase shifting and the voltage drop across the inductor can be ignored, which gives $v_g \approx v_c$. Hence, the base voltage v_o can be chosen equal to the grid voltage v_g, resulting in the following controller:

$$v = v_g + (1 - w_q)(\sqrt{2} V_g \sin(\omega_g t + \delta) - wi). \tag{25}$$

This also helps with the initial connection to the grid since according to the initial condition of the controller state $w_{q0} = 1$ and $v = v_g$ before the connection with the grid. Hence, a smooth connection can be achieved. After connecting with the grid, the controller can be enabled at any time; thus, no presynchronization unit is required.

Based on the controller (25), the measured signals v_g and i are directly used in the control input v and therefore they represent feed-forwarded terms that can introduce a small phase shift due to computational delays, pulse width modulation, and the inverter filter. To overcome this small phase shift, a phase-lead low-pass filter can be used for the measurements of v_g and i, e.g., $F(s) = \frac{33(0.05s+1)}{(s+300)(0.002s+1)}$ as adopted in [1]. Since this phase shift is different in every grid-tied inverter system, the filter gain, poles, and zero can be adjusted accordingly to match the requirements of the system. In order to design the filter $F(s)$ appropriately, the simplest way is to observe the difference $v_c - v_g$ before connecting the inverter to the grid. Hence, one can tune the parameters of $F(s)$ in order to achieve $v_c - v_g = 0$ (observed using an oscilloscope). The final implementation of the controller is shown in Fig. 5.

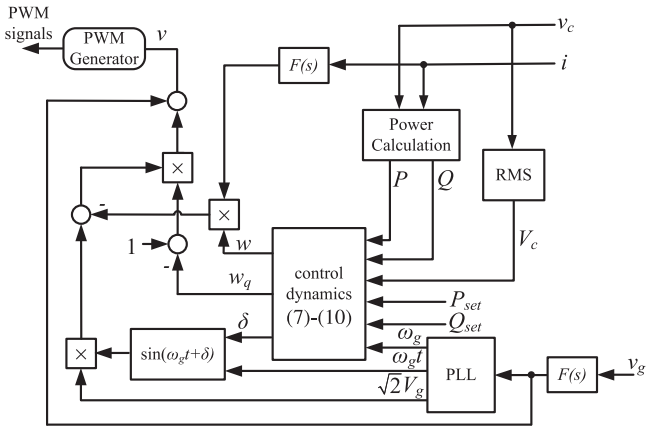

Fig. 5. Implementation diagram of the proposed controller.

IV. Operation Under Grid Variations and Faults

Since $w_{\min}$ is selected according to (18) with $V_g = E^*$, the current-limiting property is guaranteed for any $V_g \leq E^*$ and for any frequency ω_g, i.e., under grid variations (nonstiff grid) and grid faults. This is particularly interesting because, when the grid voltage drops, the current will normally increase to high values. The proposed controller is able to limit the current without changing its control structure opposed to traditional approaches which have to identify the fault and switch to a difference controller.

To further clarify this, assume that a voltage sag occurs to the grid with a percentage $p \times 100\%$, i.e., the grid voltage V_g becomes $(1-p)V_g$. Then the closed-loop system is given as

$$L\frac{di}{dt} = -(r + (1 - w_q)w)\, i + (1 - w_q)(1 - p) \times \sqrt{2} V_g \sin(\omega_g t + \delta) \tag{26}$$

which according to the same analysis for the current-limiting property yields

$$I < (1 - p) I_{\max}. \tag{27}$$

Therefore the RMS voltage of the inverter current I still remains less than $I_{\max}$, satisfying the current-limiting property and protecting the inverter. In particular, the current will try to increase forcing the controller state w to reduce to its minimum value $w_{\min}$, corresponding to the maximum allowed current independently from the droop function. When the fault is cleared, the closed-loop system becomes again as the one in (16) forcing the current i to return to its original value. Furthermore, during the fault, since $w \to w_{\min}$ then $w_q \to 0$, which results from (7) in $\dot{w} \to 0$ and the integration automatically slows down, which is an inherent antiwindup property. Hence, the proposed controller can overcome windup and latchup problems without additional switches or monitoring devices, which constitute two of the most important challenges in grid-connected inverters operation under grid faults [36]. Since the current limitation is maintained independently from the phase shift δ, the inverter is protected even if the PLL does not extract accurately the phase of the grid during faults, which is common in faulty conditions.

TABLE I
SYSTEM AND CONTROLLER PARAMETERS

Parameters	Values	Parameters	Values
L, L_g	2.2 mH	ω^*	$2\pi \times 50$ rad/s
r, r_g	0.5 Ω	ω_g	$2\pi \times 49.97$ rad/s
C	10 μF	$I_{\max}$	2 A
$V_g = E^*$	110 V	I_m	0.2 A
S_n	220 VA	K_e	150
t_s	0.1 s	k_w , k_δ	1

If $I_{\max}$ is chosen according to the ratings of the inverter, e.g., given a rated power S_n, then (27) is equivalent to

$$S < (1-p)S_n \tag{28}$$

by ignoring the small voltage drop at the filter, which provides a limit for the apparent power of the inverter at all times, even during faults.

In order to cope with possible over-voltage in the grid, the voltage V_g could be chosen as the maximum possible grid voltage when selecting $w_{\min}$.

It should be noted that the proposed controller can guarantee the current-limiting property independently from the phase shift δ or an error in the phase angle of the grid obtained by the PLL, which is critical especially under grid faults. The reason is that the current-limiting property has been mathematically proven in Section III-C to hold independently from the phase shift δ, since for the ISS property the maximum value of $|\sin(\omega_g t + \delta)|$ is required, which is equal to 1. Even if there was an error in the phase angle of the grid obtained from the PLL (possible scenario during grid faults), this error would appear as an additional component in the sinusoidal term that does not affect the current-limiting property. This is a significant advantage of the proposed controller compared to existing methods that include a PLL and introduce a current-limiting property.

V. EXPERIMENTAL RESULTS

In order to demonstrate the proposed controller, a 220 VA grid-connected single-phase inverter with an LCL filter was experimentally tested. The system and controller parameters are shown in Table I. The RMS voltage of the grid V_g is equal to the rated value E^*, and the grid frequency ω_g is slightly less than ω^* (see Table I). For the inverter droop functions, it is expected that 5% increase of the voltage should correspond to 100% decrease of the real power, and 1% increase of the frequency should correspond to 100% increase of the reactive power, since the inverter operates with a virtual resistive output impedance. Then the droop coefficients can be calculated as $n = \frac{0.05K_e E^*}{S_n}$ and $m = \frac{0.01\omega^*}{S_n}$ according to [1] and [16], where S_n is the rated power of the inverter. A switching frequency of 15 kHz was used for the inverter operation and the sinusoidal tracking algorithm (STA) was applied to obtain the required V_g and ω_g for the controller design [1]. The controller parameters c_w and c_δ are directly calculated from (23) and (24), respectively. The proposed controller was implemented using the TMS320F28335 DSP with a sampling frequency of 4 kHz.

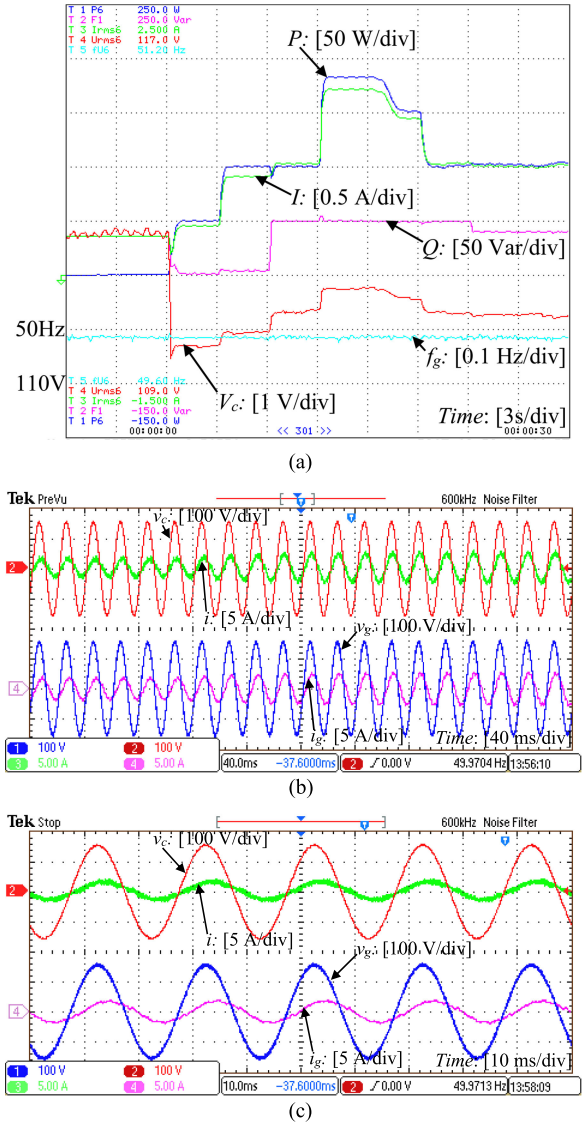

Fig. 6. Operation with a normal grid: (a) real and reactive power, RMS capacitor voltage, and inverter current and grid frequency, (b) transient response at $t = 15$ s (current-limiting property), and (c) steady-state response after 30 s.

A. Operation Under Normal Grid

Initially, a stiff grid is considered with the system parameters given in Table I. The time response of the inverter is shown in Fig. 6. It is clear that the grid frequency is constant at 49.97 Hz. The inverter is connected to the grid at $t = 6$ s and the real and reactive power references are operated in the set mode with $P_{\text{set}} = 50$ W and $Q_{\text{set}} = 0$ Var, respectively. As shown in Fig. 6(a), both the real power and the reactive power are regulated to their reference values, although the reactive power is slightly positive (less than 5 Var) due to the limitation of the power analyzer that cannot show negative reactive power and introduces small inaccuracies close to zero. At $t = 9$ s the real power reference is changed to 100 W and at $t = 12$ s the reactive power reference is changed to 50 Var. Fig. 6(a) clearly demonstrates the ability of the proposed controller to regulate

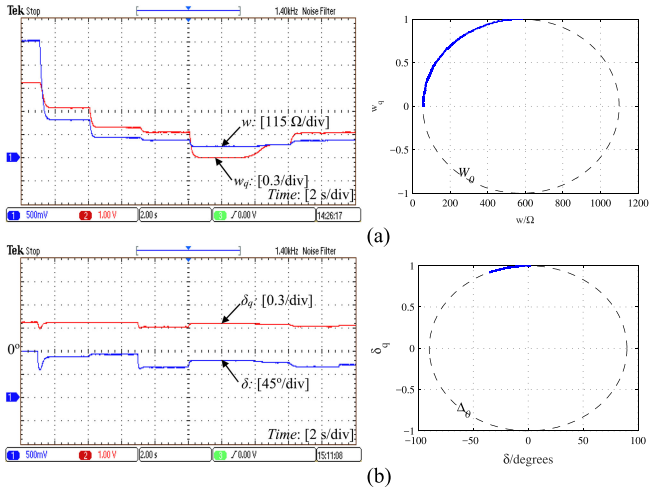

Fig. 7. Transient response of the controller states: (a) w and w_q, and (b) δ and δ_q (normal grid).

the injected power to a given level. At the time instant $t = 15$ s, the reference P_{set} is changed to 250 W, which exceeds the inverter capacity and forces the inverter current to exceed $I_{\max}$. However, as shown in Fig. 6(a), the real power is regulated at around 180 W because the current has reached the maximum allowed value. Particularly, the RMS value of the current is limited at 1.73 A. It is less than $I_{\max} = 2$ A for the following reasons: i) the parasitic resistance r of the L inductor is not zero and ii) the proposed controller uses the feed-forwarded voltage term v_g from (25) instead of v_c, which are slightly different. Nevertheless, according to the analysis and the results, the current still remains below the maximum value $I_{\max}$ as required. In practice, $I_{\max}$ can be chosen slightly larger to cover these issues. If the parasitic resistance r is known, one can choose $w_{\min} = \frac{V_g}{I_{\max}} - r$ instead of using (18), and since at the limit $w_q \to 0$, then (19) will result in this case in $|i| \leq \sqrt{2} I_{\max}$ achieving a limit for the RMS value at $I_{\max}$ and not in a smaller value. However, even if r is neglected in the control design, the inverter still stays in the safe range below the maximum current value. The transient responses of the inverter and grid currents and voltages are shown in Fig. 6(b), where the inverter current increases and reaches the maximum allowed value. At $t = 18$ s, P_{set} is changed to 150 W and in order to check the droop functions of the proposed controller, at $t = 21$ s, the $P \sim V$ droop function is enabled and the real power drops in order to bring the capacitor voltage V_c closer to the rated value E^*. This is clearly observed in Fig. 6(a). Finally, at $t = 23$ s, the $Q \sim -\omega$ droop function is enabled and the reactive power drops since the system frequency is lower than the rated value. This verifies the capability of the controller to operate in both the set mode and the droop mode. The steady-state response of the system is shown in Fig. 6(c).

To verify the analysis presented in Section III, the responses of the controller states w, w_q and δ, δ_q as shown in Fig. 7(a) and (b), respectively. The phase planes of w, w_q and δ, δ_q verify that the controller states are restricted on the upper semiellipse of W_0 and Δ_0, respectively, during the whole operation.

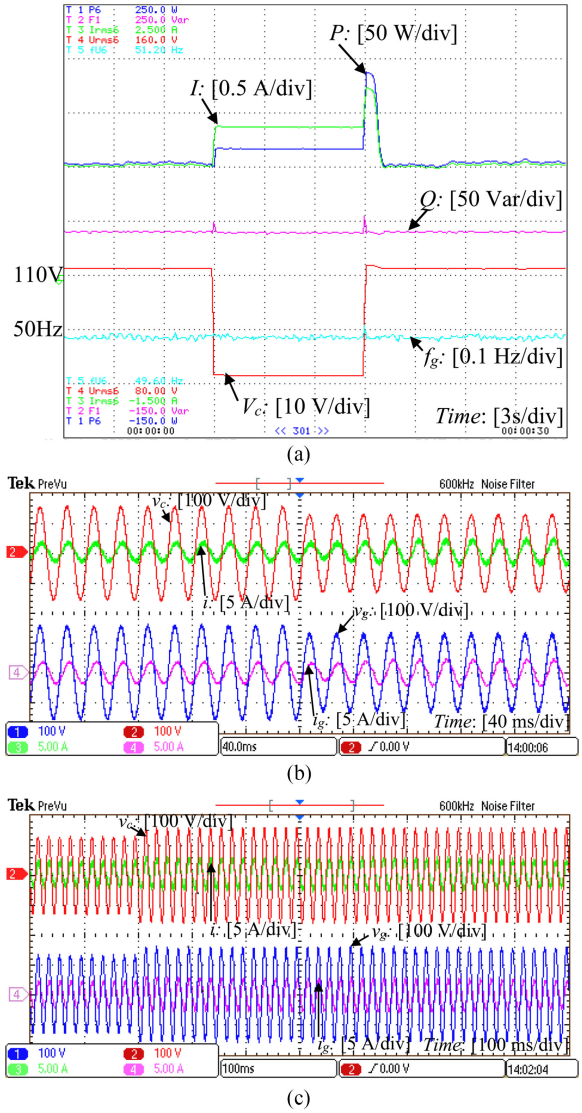

Fig. 8. Operation under grid voltage sag (110 V → 90 V): (a) real and reactive power, RMS capacitor voltage, and inverter current and grid frequency, (b) transient response when the fault occurs, and (c) transient response when the fault is cleared.

B. Operation Under Grid Faults

To further validate the current-limiting control performance, two different cases of grid voltage sags were investigated while the inverter remains in the droop mode.

At first, the grid voltage drops rapidly from 110 to 90 V and the fault is cleared after 9 s. During the fault, the current tries to increase but is eventually limited according to the current-limiting property of the controller, as shown in Fig. 8(a) and (b). Based on (27) and the percentage of the voltage drop ($p = \frac{110-90}{110} \times 100\% = 18.2\%$), the maximum RMS current would be $0.818 I_{\max} = 1.64$ A. From Fig. 8(a), it is clear that the current is limited at around 1.4 A, slightly lower than the limit due to the reasons mentioned in the previous section. Fig. 8(b) indicates the drop of the grid voltage and the capacitor voltage and the smooth increase of the current. When the fault is

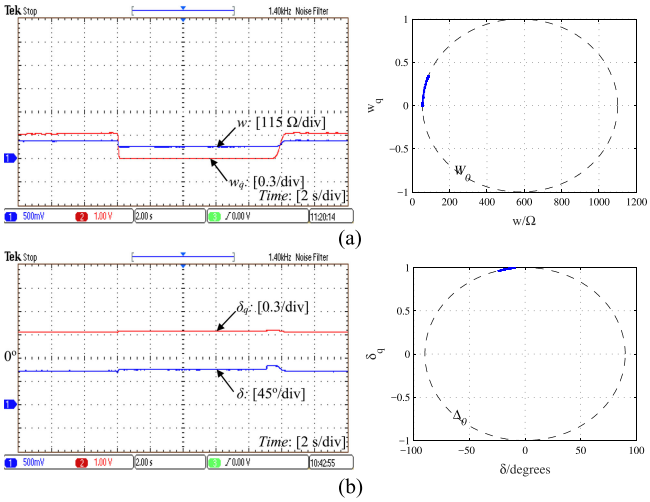

Fig. 9. Transient response of the controller states: (a) w and w_q, and (b) δ and δ_q (grid voltage sag 110 V → 90 V).

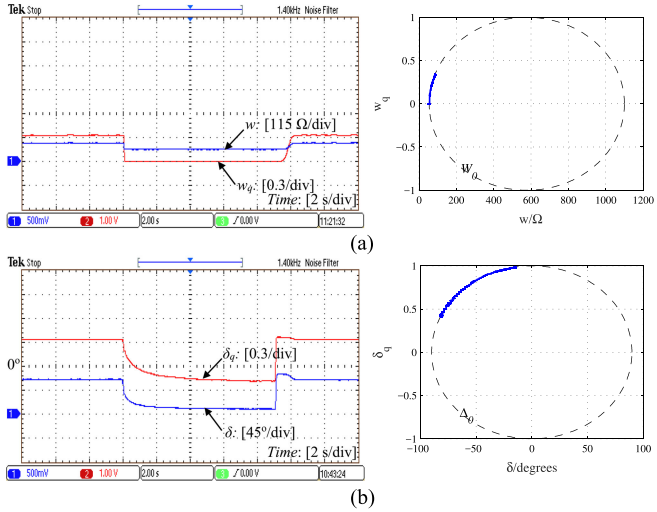

Fig. 11. Transient response of the controller states: (a) w and w_q, and (b) δ and δ_q (grid voltage sag 110 V → 55 V).

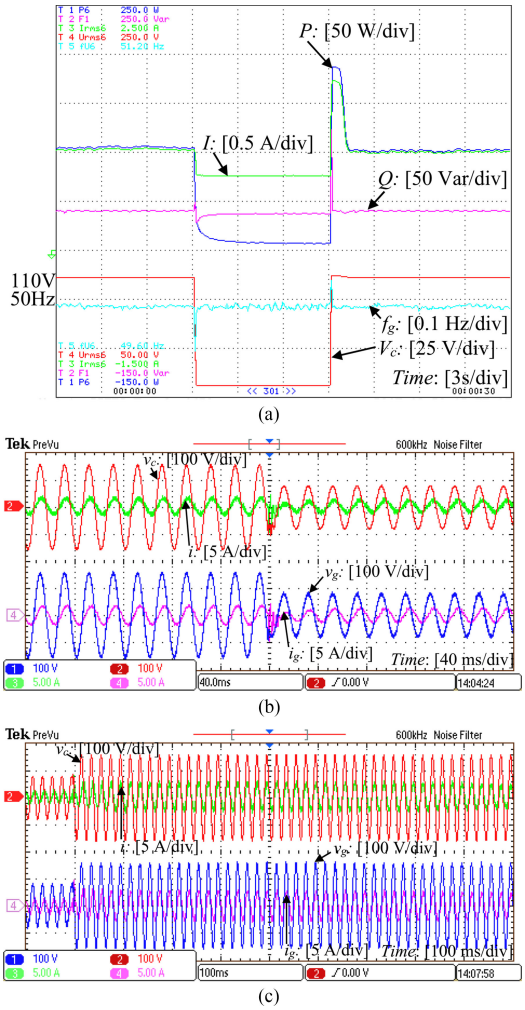

Fig. 10. Operation under grid voltage sag (110 V → 55 V): (a) real and reactive power, RMS capacitor voltage, and inverter current and grid frequency, (b) transient response when the fault occurs, and (c) transient response when the fault is cleared.

cleared, the system returns to its initial operation after a short transient [see Fig. 8(a) and (c)]. This transient is caused due to the fact that the controller state w, which represents the main part of the virtual resistance, is regulated at $w_{\min}$ for the duration of the fault. Then, when the grid voltage rapidly increases, the current will increase due to the small resistance $w_{\min}$ but it never violates the limit as rigorously proven in the theory. This is clearly shown in the time response of the controller states w and w_q in Fig. 9(a). Nevertheless, the inverter voltage is immediately restored close to the rated value after a fault clearance, as required by the Grid Code [41]. Since the frequency of the grid remains constant and (28) is not violated according to the given $Q_{\text{set}} = 50$ Var and the droop control, the reactive power is regulated at the same value during the fault [see Fig. 8(a)], which is achieved from the performance of the controller states δ and δ_q [see Fig. 9(b)]. The controller state trajectories remain again on the desired upper ellipses on the $w - w_q$ and $\delta - \delta_q$ planes.

In the second scenario, the grid voltage drops rapidly from 110 to 55 V (50% voltage sag) and returns to its original value after 9 s [see Fig. 10(a)]. In this case, the inverter current reduces since it is limited below 1 A and the real power drops during the fault to protect the system. This is shown in Fig. 10(b). As in the previous grid fault scenario, when the fault is cleared, the system returns to its initial operation after a short transient [see Fig. 10(c)]. Some oscillations, which are caused by the slow response of the PLL and the dynamics of the LCL filter, appear in the inverter current and capacitor voltage during the fault and during its clearance since for simplicity the controller (25) was used instead of its initial form (6). However, this transient only lasts for less than a half cycle with limited amplitude, which is acceptable in practice. A difference between this and the previous fault scenario is that during the fault and the current limitation (28), the droop control in the reactive power can no longer be accomplished with the given $Q_{\text{set}} = 50$ Var. This means that the controller states δ and δ_q also decrease and

converge to lower values that correspond to a lower reactive power that guarantees (28). This is shown in the time response of the controller states in Fig. 11(b). Finally, both pairs w, w_q and δ, δ_q remain on the ellipses as imposed by the theory.

VI. Conclusion

A nonlinear droop controller with a current-limiting property was proposed for single-phase grid-connected inverters. In addition to achieving the desired droop functions with a tight regulation of the output voltage close to the rated value or accurate real and reactive power regulation in the set mode, the proposed controller was able to limit the inverter current under normal or faulty grid conditions. Based on the nonlinear dynamics of the system and using input-to-state stability theory, detailed stability analysis of the control system was provided. The desired performance of the proposed controller was verified with extensive experimental results.

It has been noticed that during the fault, the proposed controller shows some oscillations due to the PLL dynamics and also the current is limited to a value lower than the given maximum value because of the grid voltage drop. Future research will focus on the investigation of controller design and stability without a PLL, on the comparison with control methods equipped with nested loops, and also on the control design to fully utilize the capability of the inverter in terms of the maximum current and power.

References

[1] Q.-C. Zhong and T. Hornik, *Control of Power Inverters in Renewable Energy and Smart Grid Integration*. Hoboken, NJ, USA: Wiley, 2013.

[2] Q.-C. Zhong and G. Weiss, "Synchronverters: Inverters that mimic synchronous generators," *IEEE Trans. Ind. Electron.*, vol. 58, no. 4, pp. 1259–1267, Apr. 2011.

[3] J. M. Guerrero, J. Matas, L. G. de Vicuna, M. Castilla, and J. Miret, "Decentralized control for parallel operation of distributed generation inverters using resistive output impedance," *IEEE Trans. Ind. Electron.*, vol. 54, no. 2, pp. 994–1004, Nov. 2007.

[4] I. Sadehkhani, M. E. H. Golshan, J. M. Guerrero, and A. Mehrizi-Sani, "A current limiting strategy to improve fault ride-through of inverter interfaced autonomous microgrids," *IEEE Trans. Smart Grid*, to be published, doi: 10.1109/TSG.2016.2517201.

[5] Q.-C. Zhong and Y. Zeng, "Can the output impedance of an inverter be designed capacitive?" in *Proc. 37th Annu. IEEE Conf. Ind. Electron.*, Nov. 2011, pp. 1220–1225.

[6] Q. C. Zhong and Y. Zeng, "Universal droop control of inverters with different types of output impedance," *IEEE Access*, vol. 4, pp. 702–712, Jan. 2016.

[7] T. L. Vandoorn, J. D. M. De Kooning, B. Meersman, J. M. Guerrero, and L. Vandevelde, "Automatic power-sharing modification of *P/V* droop controllers in low-voltage resistive microgrids," *IEEE Trans. Power Del.*, vol. 27, no. 4, pp. 2318–2325, Oct. 2012.

[8] T. L. Vandoorn, J. D. M. DeKooning, B. Meersman, and L.Vandevelde, "Review of primary control strategies for islanded microgrids with power-electronic interfaces," *Renew. Sustain. Energy Rev.*, vol. 19, pp. 613–628, 2013.

[9] J. Guerrero, L. Hang, and J. Uceda, "Control of distributed uninterruptible power supply systems," *IEEE Trans. Ind. Electron.*, vol. 55, no. 8, pp. 2845–2859, Aug. 2008.

[10] Q.-C. Zhong and Y. Zeng, "Control of inverters via a virtual capacitor to achieve capacitive output impedance," *IEEE Trans. Power Electron.*, vol. 29, no. 10, pp. 5568–5578, Oct. 2014.

[11] J. Guerrero, M. Chandorkar, T. Lee, and P. Loh, "Advanced control architectures for intelligent microgrids-Part I: Decentralized and hierarchical control," *IEEE Trans. Ind. Electron.*, vol. 60, no. 4, pp. 1254–1262, Apr. 2013.

[12] H. Komurcugil, S. Ozdemir, I. Sefa, N. Altin, and O. Kukrer, "Sliding-mode control for single-phase grid-connected LCL-filtered VSI with double-band hysteresis scheme," *IEEE Trans. Ind. Electron.*, vol. 63, no. 2, pp. 864–873, Feb. 2016.

[13] M. Karimi-Ghartemani, "Universal integrated synchronization and control for single-phase dc/ac converters," *IEEE Trans. Power Electron.*, vol. 30, no. 3, pp. 1544–1557, Mar. 2015.

[14] H. Avelar, W. Parreira, J. Vieira, L. de Freitas, and E. A. Coelho, "A state equation model of a single-phase grid-connected inverter using a droop control scheme with extra phase shift control action," *IEEE Trans. Ind. Electron.*, vol. 59, no. 3, pp. 1527–1537, Mar. 2012.

[15] J. Vasquez, J. Guerrero, A. Luna, P. Rodriguez, and R. Teodorescu, "Adaptive droop control applied to voltage-source inverters operating in grid-connected and islanded modes," *IEEE Trans. Ind. Electron.*, vol. 56, no. 10, pp. 4088–4096, Oct. 2009.

[16] Q.-C. Zhong, "Robust droop controller for accurate proportional load sharing among inverters operated in parallel," *IEEE Trans. Ind. Electron.*, vol. 60, no. 4, pp. 1281–1290, Apr. 2013.

[17] M. A. Abusara, S. M. Sharkh, and J. M. Guerrero, "Improved droop control strategy for grid-connected inverters," *Sustain. Energy, Grids Netw.*, vol. 1, pp. 10–19, 2015.

[18] R. Majumder, "Some aspects of stability in microgrids," *IEEE Trans. Power Syst.*, vol. 28, no. 3, pp. 3243–3252, Aug. 2013.

[19] X. Tang, W. Deng, and Z. Qi, "Investigation of the dynamic stability of microgrid," *IEEE Trans. Power Syst.*, vol. 29, no. 2, pp. 698–706, Mar. 2014.

[20] R. Majumder, B. Chaudhuri, A. Ghosh, G. Ledwich, and F. Zare, "Improvement of stability and load sharing in an autonomous microgrid using supplementary droop control loop," *IEEE Trans. Power Syst.*, vol. 25, no. 2, pp. 796–808, May 2010.

[21] Y. Mohamed and E. El-Saadany, "Adaptive decentralized droop controller to preserve power sharing stability of paralleled inverters in distributed generation microgrids," *IEEE Trans. Power Electron.*, vol. 23, no. 6, pp. 2806–2816, Nov. 2008.

[22] G. Konstantopoulos, Q.-C. Zhong, B. Ren, and M. Krstic, "Bounded droop controller for parallel operation of inverters," *Automatica*, vol. 53, pp. 320–328, 2015. [Online]. Available: http://dx.doi.org/http://dx.doi.org/10.1016/j.automatica.2015.01.012

[23] J. Schiffer, R. Ortega, A. Astolfi, J. Raisch, and T. Sezi, "Conditions for stability of droop-controlled inverter-based microgrids," *Automatica*, vol. 50, no. 10, pp. 2457–2469, 2014.

[24] J. W. Simpson-Porco, F. Dörfler, and F. Bullo, "Synchronization and power sharing for droop-controlled inverters in islanded microgrids," *Automatica*, vol. 49, no. 9, pp. 2603–2611, 2013.

[25] Q.-C. Zhong and G. C. Konstantopoulos, "Nonlinear current-limiting control for grid-tied inverters," in *Proc. 2016 Amer. Control Conf.*, Boston, MA, USA, Jul. 6–8, 2016, pp. 7472–7477.

[26] J. Schiffer, D. Zonetti, R. Ortega, A. Stankovic, T. Sezi, and J. Raisch, "A survey on modeling of microgrids—From fundamental physics to phasors and voltage sources," *Automatica*, vol. 74, pp. 135–150, 2016.

[27] H. Yazdanpanahi, Y. W. Li, and W. Xu, "A new control strategy to mitigate the impact of inverter-based DGs on protection system," *IEEE Trans. Smart Grid*, vol. 3, no. 3, pp. 1427–1436, Sep. 2012.

[28] D. M. Vilathgamuwa, P. C. Loh, and Y. Li, "Protection of microgrids during utility voltage sags," *IEEE Trans. Ind. Electron.*, vol. 53, no. 5, pp. 1427–1436, Oct. 2006.

[29] H. J. Laaksonen, "Protection principles for future microgrids," *IEEE Trans. Power Electron.*, vol. 25, no. 12, pp. 2910–2918, Dec. 2010.

[30] X. Guo, W. Liu, X. Zhang, X. Sun, Z. Lu, and J. M. Guerrero, "Flexible control strategy for grid-connected inverter under unbalanced grid faults without PLL," *IEEE Trans. Power Electron.*, vol. 30, no. 4, pp. 1773–1778, Apr. 2015.

[31] M. A. Haj-ahmed and M. S. Illindala, "The influence of inverter-based DGs and their controllers on distribution network protection," *IEEE Trans. Ind. Appl.*, vol. 50, no. 4, pp. 2928–2937, Jul./Aug. 2014.

[32] H. H. Zeineldin, E. F. El-Saadany, and M. M. A. Salama, "Protective relay coordination for micro-grid operation using particle swarm optimization," in *Proc. 2006 Large Eng. Syst. Conf. Power Eng.*, Halifax, NS, Canada, Jul. 26–28, 2006, pp. 152–157.

[33] Y. Yang, F. Blaabjerg, and H. Wang, "Low-voltage ride-through of single-phase transformerless photovoltaic inverters," *IEEE Trans. Ind. Appl.*, vol. 50, no. 3, pp. 1942–1952, May/Jun. 2014.

[34] M. S. El Moursi, W. Xiao, and J. L. Kirtley, "Fault ride through capability for grid interfacing large scale PV power plants," *IET Gener., Transmiss. Distrib.*, vol. 7, no. 9, pp. 1027–1036, 2013.

[35] A. D. Paquette and D. M. Divan, "Virtual impedance current limiting for inverters in microgrids with synchronous generators," *IEEE Trans. Ind. Appl.*, vol. 51, no. 2, pp. 1630–1638, Mar./Apr. 2015.
[36] N. Bottrell and T. C. Green, "Comparison of current-limiting strategies during fault ride-through of inverters to prevent latch-up and wind-up," *IEEE Trans. Power Electron.*, vol. 29, no. 7, pp. 3786–3797, Jul. 2014.
[37] H. Xin, L. Huang, L. Zhang, Z. Wang, and J. Hu, "Synchronous instability mechanism of P-f droop-controlled voltage source converter caused by current saturation," *IEEE Trans. Power Syst.*, vol. 31, no. 6, pp. 5206–5207, Nov. 2016.
[38] G. C. Konstantopoulos, Q.-C. Zhong, and W.-L. Ming, "PLL-less nonlinear current-limiting controller for single-phase grid-tied inverters: Design, stability analysis and operation under grid faults," *IEEE Trans. Ind. Electron.*, vol. 63, no. 9, pp. 5582–5591, Sep. 2016.
[39] G. C. Konstantopoulos, Q.-C. Zhong, B. Ren, and M. Krstic, "Bounded integral control of input-to-state practically stable non-linear systems to guarantee closed-loop stability," *IEEE Trans. Autom. Control*, to be published, doi: 10.1109/TAC.2016.2552978.
[40] H. K. Khalil, *Nonlinear Systems*. Englewood Cliffs, NJ, USA: Prentice-Hall, 2001.
[41] *The Grid Code*. National Grid Electricity Transmission plc, London, U.K., 2016.

Qing-Chang Zhong (M'03–SM'04–F'17) received the Ph.D. degree in control and power engineering from Imperial College London, London, U.K., in 2004 (awarded the Best Doctoral Thesis Prize), and the Ph.D. degree in control theory and engineering from Shanghai Jiao Tong University, Shanghai, China, in 2000.

He is the Max McGraw Endowed Chair Professor in energy and power engineering at the Department of Electrical and Computer Engineering, Illinois Institute of Technology, Chicago, IL, USA.

Prof. Zhong is a Distinguished Lecturer of the IEEE Power and Energy Society, IEEE Power Electronics Society, and IEEE Control Systems Society. He is a Fellow of the Institution of Engineering and Technology (IET), U.K., and the Vice-Chair of the IFAC Technical Committee on Power and Energy Systems, and was a Senior Research Fellow of the Royal Academy of Engineering, U.K. (2009–2010), and the U.K. Representative to the European Control Association (2013–2015). He serves as an Associate Editor of the IEEE TRANSACTIONS ON AUTOMATIC CONTROL, IEEE TRANSACTIONS ON INDUSTRIAL ELECTRONICS, IEEE TRANSACTIONS ON POWER ELECTRONICS, IEEE TRANSACTIONS ON CONTROL SYSTEMS TECHNOLOGY, IEEE ACCESS, and IEEE JOURNAL OF EMERGING AND SELECTED TOPICS IN POWER ELECTRONICS.

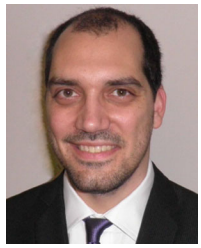

George C. Konstantopoulos (S'07–M'13) received the Diploma and Ph.D. degrees in electrical and computer engineering from the Department of Electrical and Computer Engineering, University of Patras, Rion, Greece, in 2008 and 2012, respectively.

From 2011 to 2012, he was an Electrical Engineer with the Public Power Corporation of Greece. Since 2013, he has been with the Department of Automatic Control and Systems Engineering, The University of Sheffield, Sheffield, U.K., initially as a Postdoctoral Researcher and currently as a Lecturer. His research interests include nonlinear modeling, control and stability analysis of power converters in microgrid and smart grid applications, renewable energy systems, and electrical drives.

Dr. Konstantopoulos is a member of the National Technical Chamber of Greece.